

X-ray Study on the Nature of the Colliding Stellar Winds in the Massive Star Binary WR140

Manabu Ishida,^{a,b,*} Asca Miyamoto,^b Yoshitomo Maeda,^a Kenji Hamaguchi,^{c,d} Yasushi Sugawara,^a Michael Corcoran,^c Christopher Russel^e and Anthony Moffat^f

^a*Institute of Space and Astronautical Science/JAXA, 3-1-1 Chuo, Sagami-hara, Kanagawa 252-5210, Japan*

^b*Faculty of Science, Tokyo Metropolitan University, 1-1 Minami-Osawa, Hachioji, Japan*

^c*CRESST II and X-ray Astrophysics Laboratory NASA/GSFC, Greenbelt, MD 20771, USA*

^d*Department of Physics, University of Maryland, Baltimore County, 1000 Hilltop Circle, Baltimore, MD 21250, USA*

^e*Department of Physics and Astronomy, Bartol Research Institute, University of Delaware, Newark, DE 19716 USA*

^f*Département de physique and Centre de Recherche en Astrophysique du Québec (CRAQ), Université de Montréal, CP 6128, Montréal, Canada*

*E-mail: ishida@astro.isas.jaxa.jp, miyamoto-asuka@ed.tmu.ac.jp,
yamaeda@astro.isas.jaxa.jp, kenjih@umbc.edu, yasu_hare@yahoo.co.jp,
michael.f.corcoran@nasa.gov, crussell@udel.edu, moffat@astro.umontreal.ca*

We analysed *XMM-Newton* RGS data of the colliding-wind massive star binary WR140 taken over 8 years. From the line-of-sight velocity of Ne $K\alpha$ lines, we derived the distance of the Ne line-emission region from the stagnation point of the shock cone. We performed diagnostics of the electron number density with the He-like triplet of the Ne $K\alpha$ line.

Multifrequency Behaviour of High Energy Cosmic Sources XIV (MULTIF2023)
12-17 June 2023
Palermo, Italy

*Speaker

1. Introduction

Wolf-Rayet 140 (WR140) is a massive star binary composed of a WR star and an O star whose spectral types are WC7pd and O5.5fc [1], respectively, orbiting each other with a period of nearly 8 years. Figure 1 shows a schematic view of the WR140 binary system. Both stars expel massive

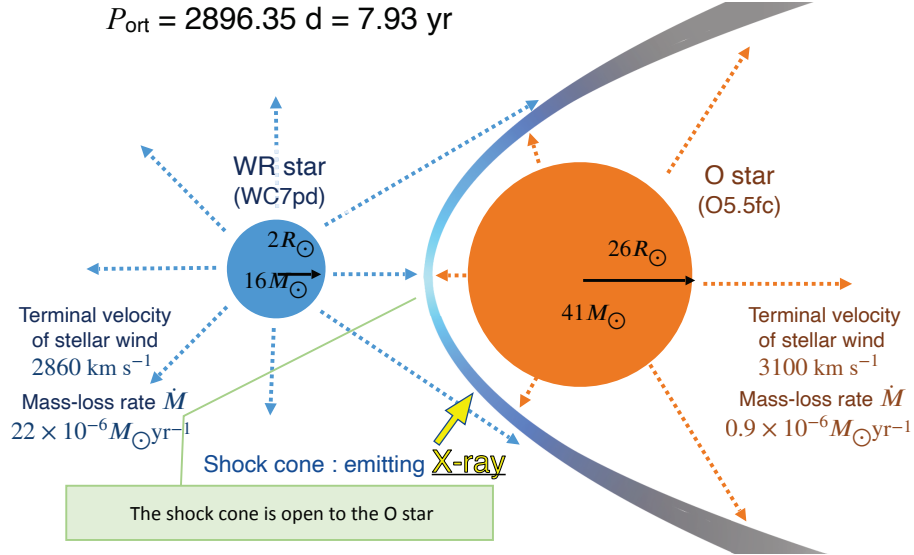


Figure 1: Schematic view of the WR140 binary.

high-velocity stellar winds, which are highly supersonic, and hence their collision forms a shock cone where the wind matter is compressed and heated up into a hot plasma emitting X-rays. Ram pressure of the WR star's wind is greater, so the cone bends toward the O star. We refer the readers to [2, 3] for the binary parameters.

2. Observations

We have analysed data of the Reflection Grating Spectrometer (RGS) [4] onboard XMM-Newton [5]. The observation log can be found in table 3 of [6]. We have analysed in total 10 datasets which cover the entire 8 years orbit. Figure 2 shows how the 10 observations distribute in the O-star's orbit. In this figure, the WR star is fixed at one of the foci of the O-star's elliptical orbit. The observer views the binary along the dashed line which is elevated from the paper by $\approx 60^\circ$. Note that the inferior conjunction of the O star occurs between phase L (0.935) and B (0.968).

Figure 3 summarizes the spectra from the 10 orbital phases in the band 0.3-2 keV. WR140 is bright enough at phases K (0.816), A (0.912), L (0.935), B (0.968), and D (0.987). At these phases, the observer is inside the shock cone, viewing the system from the O star's side. For subsequent analysis, we concentrate on the data from these five bright phases.

3. Aim of our research

Figure 4 shows the RGS spectra of WR140 at Phase-A (0.912). The spectra are characterized

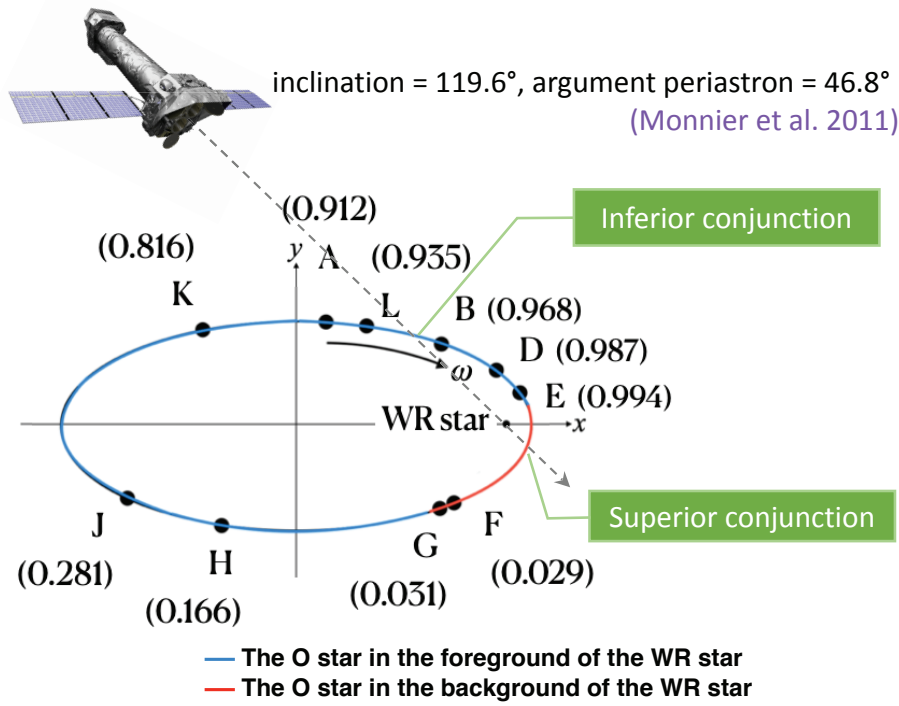


Figure 2: Schematic view of the WR140 orbit. The orbital phase 0 means the periastron of the binary. The WR star is fixed at one of the foci of the O-star's elliptical orbit. Note that the the observer views the binary along the dashed line which is elevated from the paper by ≈ 60 degrees. The inferior conjunction of the O star occurs between phase L (0.935) and B (0.968).

with K-lines of hydrogenic and He-like Oxygen and Neon, as well as L-lines of Fe. Using the spectra also from the other X-ray-bright phases, we aim to understand the state of the wind-collision plasma with the following methods.

1. We measure the line-of-sight velocity and its dispersion of the plasma with the energy shift and the line broadening.
2. In parallel, we calculate the shape of the shock cone and plasma velocity along the cone, in order to identify the location of the line-emission sites on the shock cone.
3. We can measure the densities along the shock cone with the He-like triplet lines.

In this presentation, we will mainly report on the results on the Ne lines. We refer the readers to [6] and Miyamoto et al. (2023) recently accepted for publication in Monthly Notices of the Royal Astronomical Society.

4. Analyses

4.1 Line-of-sight velocity and its dispersion

First, we have carried out a model fitting to the spectra to derive parameters of the Ne emission lines. We use energy bands near the He-like and H-like Ne $K\alpha$ lines, and have performed a

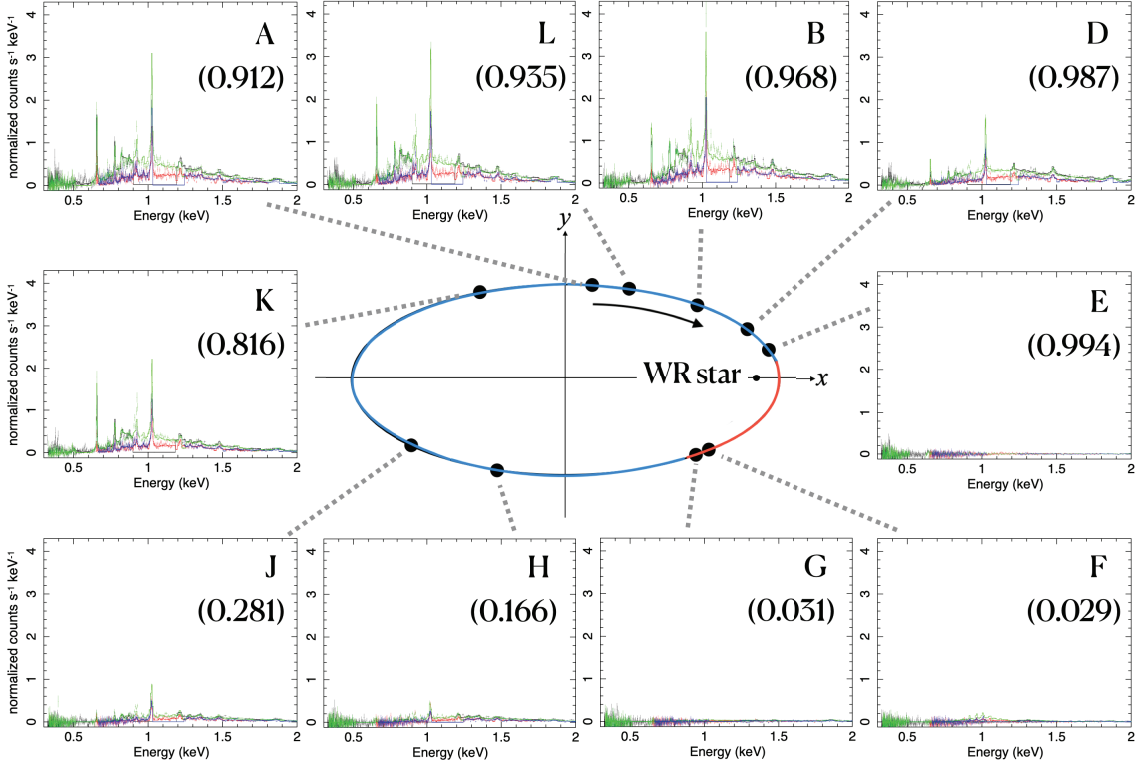


Figure 3: Spectral gallery of WR140 from the 10 RGS observations (taken from Fig. 2 of [6]).

fitting with the model `BVVAPEC`, which is an optically thin thermal plasma emission model with Doppler broadening of the lines, multiplied by the model `TBABS` which represents the photoelectric absorption by cold matter. From this fit we can obtain the plasma temperature, line-of-sight velocity and its dispersion of the Ne lines. We carry out the same fitting at all phases K (0.816), A (0.912), L (0.935), B (0.968) and D (0.987).

The results are summarized in table 5 and Fig. 4 of [6]. The plasma temperature measured with hydrogenic and He-like Ne $K\alpha$ line (= ionization temperature of Ne) ranges from 0.45-0.84 keV, depending upon the orbital phase. The line-of-sight velocity of the Ne emission line and its dispersion distribute in the ranges -600 to $-1,200$ km s^{-1} and 400 to 700 km s^{-1} , respectively. We have also carried out similar analyses on the oxygen $K\alpha$ lines and the iron L-lines. The results are plotted in Fig. 5 as a function of the orbital phase. We find all line-of-sight velocities are negative, indicating the line-emission sites are approaching us, and the maximum blueshift seems to occur between phases L (0.935) and B (0.968). The velocity dispersions seem to show their minima at around the same orbital phase. As we have mentioned in §2 with Fig. 2, the O star's inferior conjunction occurs between phases L (0.935) and B (0.968). At this phase, the observer views the system closest to the shock cone-axis from the O-star's side. Accordingly, we expect the line-of-sight velocities show their maximum blueshift, and the dispersions of the line-of-sight velocities are at their minimum. These agreements of the observational results with the expectations support the shock cone geometry shown in Fig. 1, and the shocked plasma flows basically along the shock cone.

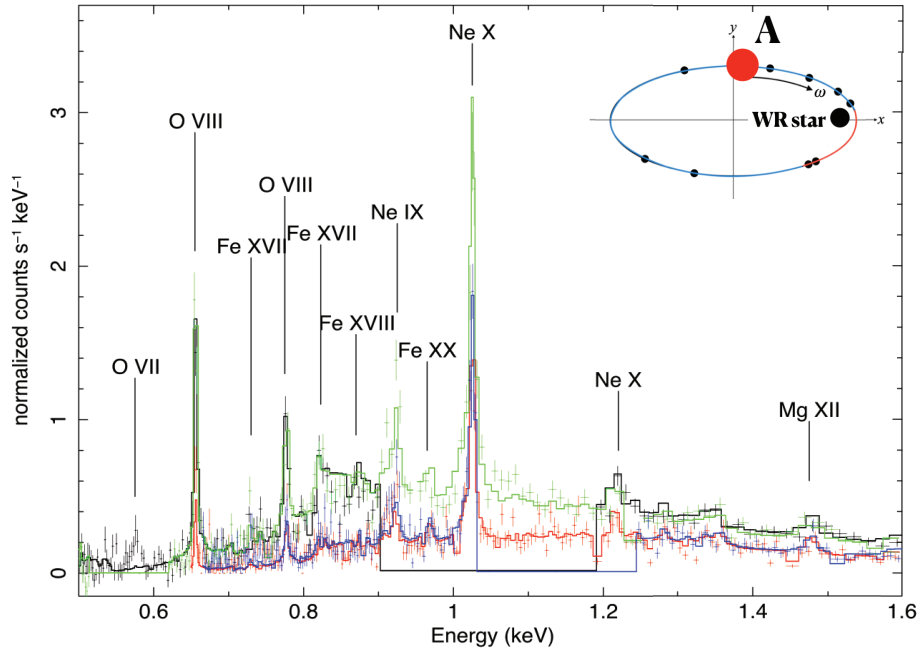


Figure 4: The RGS spectra of WR140 at Phase A (0.912) as a representative, taken from Fig. 3 of [6]. . Black and red colors represent the first order spectrum of the RGS1 and RGS2, respectively. Green and blue are assigned to the second order spectrum of RGS1 and RGS2, respectively. Hydrogenic and He-like $K\alpha$ lines from O and Ne, and L-lines of Fe dominate the spectra.

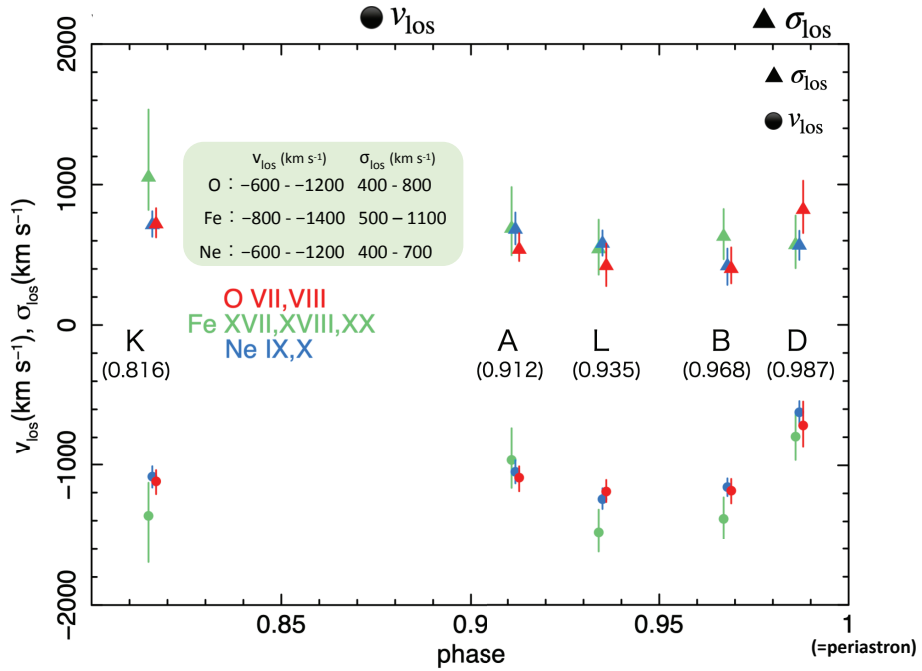


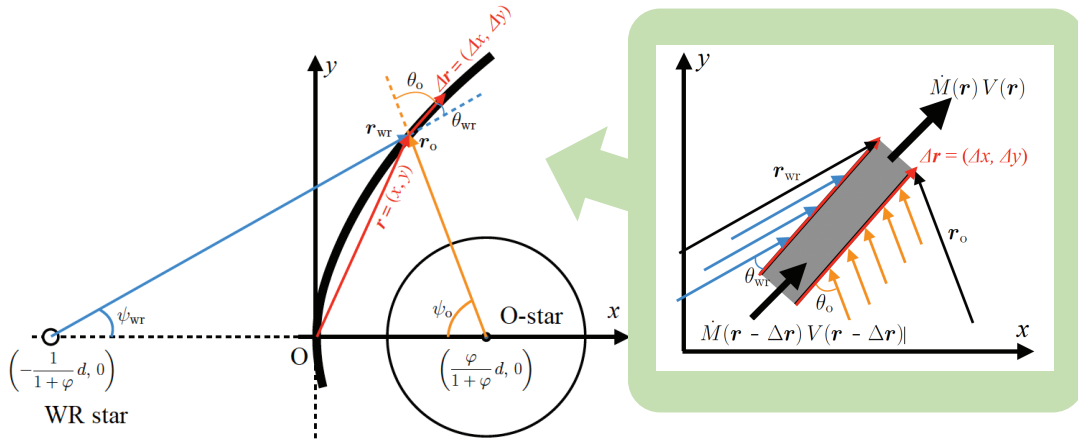
Figure 5: Line-of-sight velocities and their dispersions versus the orbital phase.

4.2 Location of the Ne line-emission site

Next, we compare the observed line-of-sight velocities with the theoretical ones to identify the location of the line-emission site on the shock cone. Again, we concentrate on the Ne emission lines. In doing this, we first derive the shape of the shock cone, which can be solved with ram-pressure balance of the stellar winds from the two component stars, based on the mass-loss rates [1, 3, 7], the velocity profile, and the terminal velocity of the winds [8, 9]. We refer the readers to §§4.1.1 through 4.1.3 of [6] for the calculation procedure in detail.

The results of the shock cone shape at the five orbital phases are shown in Fig. 8 of [6]. In that figure, the coordinates x and y are normalized by the binary separation, and written as ξ and η , respectively. The shape of these non-dimensional shock cones is almost identical among the phases, but with a slight decrease in the opening angle of the cone as the binary separation decreases. This is because the shock cone is formed before the acceleration of the O star's wind completes.

Given the shock cone shape, we next move onto calculating the plasma flow velocity along the shock cone. Figure 6 shows the calculation scheme. We consider the small plasma segment $\Delta \mathbf{r}$



- The plasma segment $\Delta \mathbf{r}$ receives the tangential component of momentum from the the stellar winds.

$$\dot{M}(\mathbf{r})V(\mathbf{r}) = \dot{M}(\mathbf{r}-\Delta\mathbf{r})V(\mathbf{r}-\Delta\mathbf{r}) + \dot{M}_{\text{wr}} \frac{\Delta\Omega_{\text{wr}}(r_{\text{wr}})}{4\pi} v_{\text{wr}}(r_{\text{wr}}) \cos\theta_{\text{wr}} + \dot{M}_{\text{o}} \frac{\Delta\Omega_{\text{o}}(r_{\text{o}})}{4\pi} v_{\text{o}}(r_{\text{o}}) \cos\theta_{\text{o}},$$

$v(r)\cos\theta$: The tangential components of stellar winds from each star.

$\Delta\Omega(r)$: The solid angle subtended by the annulus containing the vector $\Delta \mathbf{r}$ over each star.

Figure 6: Scheme of calculating the plasma flow velocity along the shock cone.

along the shock cone. The blow-up shows the segment of the shock cone around $\Delta \mathbf{r}$. The plasma at $\mathbf{r}-\Delta \mathbf{r}$ receives the tangential component of the stellar wind momentum while it passes through the segment $\Delta \mathbf{r}$ according to the equation in the figure, where $v \cos \theta$ is the tangential component of the stellar wind from each star, and $\Delta\Omega$ is the solid angle subtended by the annulus containing $\Delta \mathbf{r}$ over each star. $\dot{M}(\mathbf{r})$ is the total mass flowing into the shock cone within \mathbf{r} from the two stars

per unit time. Namely,

$$\begin{aligned}\dot{M}(\mathbf{r}) &= \dot{M}_{\text{wr}} \frac{\Omega_{\text{wr}}(\mathbf{r})}{4\pi} + \dot{M}_o \frac{\Omega_o(\mathbf{r})}{4\pi} \\ &= \frac{\dot{M}_{\text{wr}}}{2} (1 - \cos \psi_{\text{wr}}) + \frac{\dot{M}_o}{2} (1 - \cos \psi_o)\end{aligned}\quad (1)$$

We can solve this set of equations for the plasma flow velocity V by providing its initial value at the stagnation point, for which we adopt the sound velocity $c_s = 8.0 \times 10^7 \text{ cm s}^{-1}$ corresponding to the plasma temperature there ($kT_s = 3.5 \text{ keV}$: [3]).

The profile of the line-of-sight velocity as a function of ξ at phase A (0.912) is shown in Fig. 7. Under the assumption that the post-shock plasma flows along the shock cone, the line-of-sight

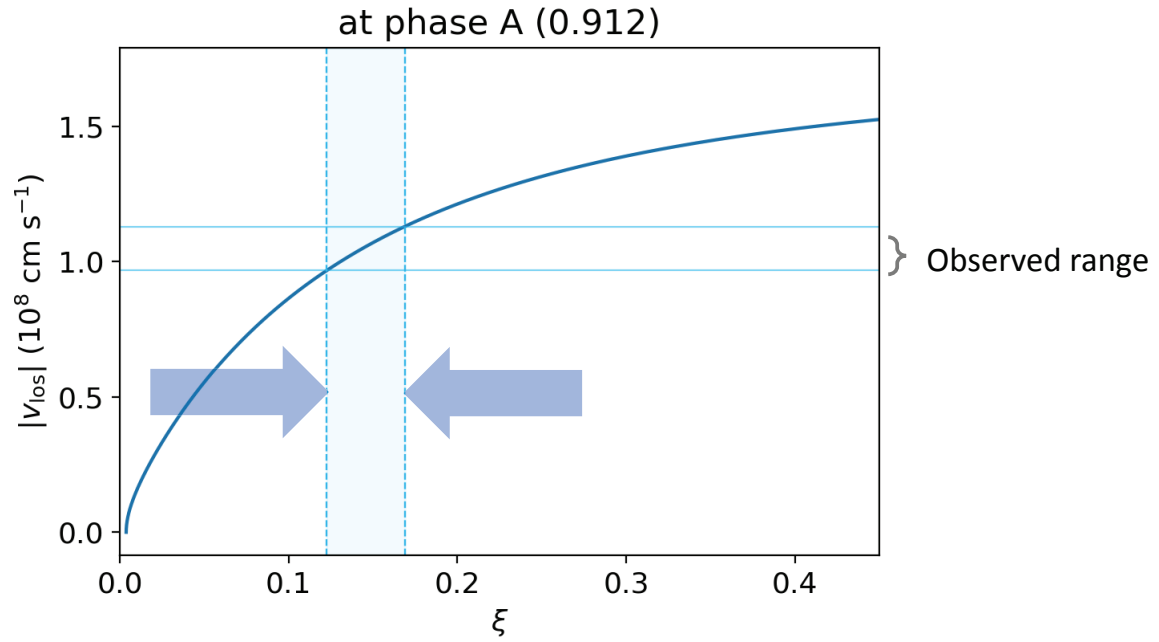


Figure 7: The profile of the line-of-sight velocity as a function of $\xi = x/d$, where d is the distance between the two component stars. This curve is utilized to measure the distance of the Ne line-emission site, indicated with the pair of the thick arrows, from the intersection of the observed range of v_{los} .

velocity can be written with orbital parameters, such as the inclination i ($= 119.6^\circ$) and argument periastron ω ($= 46.8^\circ$) as

$$v_{\text{los}}(x, y, \theta, i, \omega) = \frac{V(\mathbf{r})\Delta x}{\sqrt{(\Delta x)^2 + (\Delta y)^2}} \sin i \sin(\theta + \omega) \quad (2)$$

[6], where θ is the true anomaly, V is what we have just solved above, and $(\Delta x, \Delta y)$ is the segment $\Delta \mathbf{r}$ in Fig. 6. With this curve, we can identify the location of the Ne line-emission site from the intersection with the observed range of the line-of-sight velocities. At phase A (0.912), we find it is $(2.5\text{-}3.4) \times 10^{13} \text{ cm}$. We applied the same procedure to the other remaining phases. The distance of the Ne line-emission site ranges from $1 \times 10^{13} \text{ cm}$ [phase D (0.987)] to $13 \times 10^{13} \text{ cm}$ [phase K (0.816)].

4.3 Density of the Ne line-emission site

Finally, we estimate the electron number density of the Ne line-emission sites using intensity-ratios of the He-like triplet components of Ne. The level diagram of the He-like $K\alpha$ line can be found in Fig. 1 of [10]. The He-like $K\alpha$ line is composed of three components: a resonance line, intercombination lines and a forbidden line, which are w , $x + y$, and z in [10], respectively. Of them, the life of the upper level of the forbidden line 3S is relatively longer than the others. Hence the 3S level can be further excited to the 3P level by electron impacts, and deexcited by emitting the intercombination lines. As a result, the intercombination lines become more intense while the forbidden line becomes weaker as the plasma density increases.

We performed three Gaussian-fitting to the f ($= z$), i ($= x + y$), and r ($= w$) lines for their intensities, and compared them with the theoretical values. Here we used the f and i intensities normalized by that of r calculated with the plasma code SPEX¹. The results for phase A (0.912) is shown in Fig. 8. From The intersections of the observed ranges with the curves, we estimate the

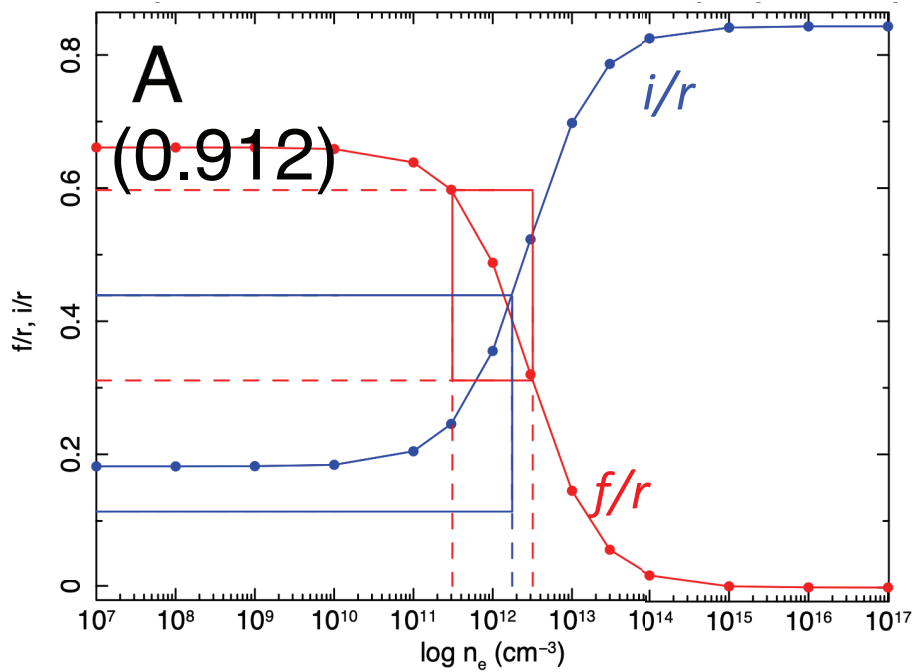


Figure 8: The line intensity ratios f/r and i/r as a function of the electron number density n_e . The red and blue boxes constrain n_e from the observed line intensity ratios.

electron number density at phase A (0.912) to be $0.3\text{--}1.8 \times 10^{12} \text{ cm}^{-3}$. The similar electron number density $n_e = 0.5\text{--}2.8 \times 10^{12} \text{ cm}^{-3}$ is obtained at phase K (0.816).

Note that the plasma in the shock cone is exposed to the intense EUV radiation from the O star, and the 3S level can be excited to the 3P level also through the photo-excitation [11]. The densities we derived here is reliable only if the collisional excitation rate is much larger than the photo-excitation rate. Accordingly, we estimated the effect of the photo-excitation by the O star's EUV radiation for all the five bright phases, and found that the rate of photo-excitation is at most

¹<https://www.sron.nl/astrophysics-splex>

9.6% of that of collisional excitation at phase K (0.816). We can therefore say that the estimated n_e at this phase is reasonably reliable. At the other phases A (0.912), L (0.935), B (0.968) and D (0.987), on the other hand, we found we need a careful evaluation of the photo-excitation. We refer the readers to [6] and references therein for the detailed calculations.

5. Summary

We analysed *XMM-Newton* RGS data of the colliding-wind massive star binary WR140 taken over 8 years. We measured the line-of-sight velocity v_{los} and its dispersion σ_{los} of the hydrogenic and He-like Ne $K\alpha$ lines, and found that the former is the most blue-shifted and the latter becomes minimum at the time of the inferior conjunction of the secondary O star. We calculated the shock cone shape from the ram-pressure balance between the stellar winds from the two component stars, and derived v_{los} as a function of the distance from the shock stagnation point. Comparing the v_{los} thus obtained to that observed, we derived the distance of the Ne line-emission region from the stagnation point of the shock cone from 1×10^{13} cm [phase D (0.987)] to 13×10^{13} cm [phase K (0.816)]. We performed diagnostics of the electron number density of the Ne line-emission site with the He-like triplet of the Ne $K\alpha$ line. We obtained $n_e = 0.5\text{-}2.8 \times 10^{12}$ cm $^{-3}$ at phase K (0.816). For the other phases, we need careful evaluation of the photo-excitation effect.

References

- [1] R. Fahed, A.F.J. Moffat, J. Zorec, T. Eversberg, A.N. Chené, F. Alves et al., *Spectroscopy of the archetype colliding-wind binary WR 140 during the 2009 January periastron passage*, *Monthly Notices of Royal Astronomical Society* **418** (2011) 2.
- [2] J.D. Monnier, M. Zhao, E. Pedretti, R. Millan-Gabet, J.P. Berger, W. Traub et al., *First Visual Orbit for the Prototypical Colliding-wind Binary WR 140*, *Astrophysical Journal Letters* **742** (2011) L1 [1111.1266].
- [3] Y. Sugawara, Y. Maeda, Y. Tsuboi, K. Hamaguchi, M. Corcoran, A.M.T. Pollock et al., *Suzaku monitoring of the Wolf-Rayet binary WR 140 around periastron passage: An approach for quantifying the wind parameters*, *Publication of Astronomical Society of Japan* **67** (2015) 121 [1509.08479].
- [4] J.W. den Herder, A.C. Brinkman, S.M. Kahn, G. Branduardi-Raymont, K. Thomsen, H. Aarts et al., *The Reflection Grating Spectrometer on board XMM-Newton*, *Astronomy and Astrophysics* **365** (2001) L7.
- [5] F. Jansen, D. Lumb, B. Altieri, J. Clavel, M. Ehle, C. Erd et al., *XMM-Newton observatory. I. The spacecraft and operations*, *Astronomy and Astrophysics* **365** (2001) L1.
- [6] A. Miyamoto, Y. Sugawara, Y. Maeda, M. Ishida, K. Hamaguchi, M. Corcoran et al., *Understanding the physical state of hot plasma formed through stellar wind collision in WR140 using high-resolution X-ray spectroscopy*, *Monthly Notices of the Royal Astronomical Society* **513** (2022) 6074 [https://academic.oup.com/mnras/article-pdf/513/4/6074/43913322/stac1289.pdf].

- [7] J.M. Pittard and S.M. Dougherty, *Radio, X-ray, and γ -ray emission models of the colliding-wind binary WR140*, *Monthly Notices of Royal Astronomical Society* **372** (2006) 801 [[astro-ph/0603787](#)].
- [8] P.M. Williams, K.A. van der Hucht, A.M.T. Pollock, D.R. Florkowski, H. van der Woerd and W.M. Wamsteker, *Multi-frequency variations of the Wolf-rayet system HD 193793 - I. Infrared, X-ray and radio observations.*, *Monthly Notices of Royal Astronomical Society* **243** (1990) 662.
- [9] D.Y.A. Setia Gunawan, K.A. van der Hucht, P.M. Williams, H.F. Henrichs, L. Kaper, D.J. Stickland et al., *Multi-frequency variations of the Wolf-Rayet system HD193793 (WC7pd+O4-5) III. IUE observations*, *Astronomy and Astrophysics* **376** (2001) 460.
- [10] D. Porquet, R. Mewe, J. Dubau, A.J.J. Raassen and J.S. Kaastra, *Line ratios for helium-like ions: Applications to collision-dominated plasmas*, *Astronomy and Astrophysics* **376** (2001) 1113 [[astro-ph/0107329](#)].
- [11] A.H. Gabriel and C. Jordan, *Interpretation of solar helium-like ion line intensities*, *Monthly Notices of Royal Astronomical Society* **145** (1969) 241.